doi.org/10.1002/batt.201900225



# Chromium Oxynitride as Durable Electrode Material for Symmetric Supercapacitors

U. Naveen Kumar,[a] Janraj Naik Ramavath,[b] Sourav Ghosh,[a, b] R. Kothandaraman,*[b] and Tiju Thomas*[a]

Recently, metal oxynitrides (MONs) have gained a lot of attention as electrode materials for supercapacitor (SC) applications due to their unique properties such as high electronic conductivity, wettability, corrosion resistance, and chemical robustness. Nanostructuring strategies of MONs opens fresh avenues for energy storage. Though various transition metal oxides (MO) and metal nitrides (MN) have been explored as electrode materials for SC applications, they have limitations associated with poor cyclability and rate capabilities. Hence, there is a value to exploring intermediate oxynitride compounds (MONs) in place of pure MOs and MNs. Chromium oxynitride ($CrO_XN_Y$) as electrode material is not yet been explored for SC applications. In this context, we have carried out the systematic study of the nanostructured nano-spherical $CrO_XN_Y$ nanoparticle as an electrode material for SC applications. The electrochemical performance of the $CrO_XN_Y$ electrode is tested in both the three and two electrode assembly. The $CrO_XN_Y$ electrode shows capacitance of 146 $F g^{-1}$ at 10 $mV s^{-1}$ in three electrode configuration. The symmetric coin cell (CR2032) is fabricated and tested up to 10,000 cycles at 2 $A g^{-1}$ and it shows excellent capacity retention up to 98%. The energy and power densities of the symmetric device are ~8 $W h kg^{-1}$ at 1 $A g^{-1}$ and 28.8 $kW kg^{-1}$ at 10 $A g^{-1}$, respectively. As a proof of concept, a red light-emitting diode (LED) is lit by serially connecting two symmetric coin cells (2 V). These attributes of $CrO_XN_Y$, such as excellent capacitance retention, long cyclic stability, and high rate capability, indicates that it can be used as a durable electrode material for SC technology.

## 1. Introduction

To fulfill the energy demands of the fast growing consumer electronics, heavy electric vehicles, and memory backups, the development of the eco-benign and sustainable energy storage/conversion devices is essential.[1] Electrochemical capacitors or supercapacitors (SCs) are of substantial utility due to their high power density, moderate energy density, fast charge-discharge rates, long cycle life (~$10^5$ cycles) and environment friendliness.[2,3] SCs are classified into electrical double layer capacitors (EDLC) and pseudocapacitors (PSC), based on the charge storage mechanism involved.[4] EDLC stores the energy through the accumulation electrostatic charges at the electrode/electrolyte interface due to non-Faradaic process.[5] On the other hand, the energy storage mechanism of PSC involves rapid redox events due to Faradaic reactions.[6]

Typically, carbonaceous materials such as activated carbons, graphenes, and carbon nanotubes (CNTs) are employed as electrode materials for EDLCs due to their high surface area and porosity.[7–9] On the other hand, electrochemically active materials such as transition metal oxides (TMO),[10,11] sulfides,[12,13] nitrides,[14] oxynitrides,[15,16] and/or conducting polymers[17] are employed as electrode materials for PSC due to their high capacitance and energy densities at least one order higher than the carbon materials. However, the poor electronic conductivity, structural degradation, and volume expansion of TMO due to Faradaic reactions eventually result in poor cyclic stability.[18]

To circumvent the above mentioned limitations, novel electrode materials with attractive properties (such as good electronic conductivity, porosity, surface area, chemical inertness, wettability and etc.) are being pursued.[19] Also, the combination of electroactive material and electrolyte used plays a crucial role in SCs technology to enhance the performance of the resulting devices.[9] Novel electrode materials with unique physicochemical properties enable ways to enhance SC technology. In spite of steady progress in the SC technology, TMO exhibits inadequate performance due to poor electrical conductivity and electrochemical stability. As an alternative to TMO, metal nitrides ($Mo_2N$, TiN, and WN) are used as electrode materials due to their chemical stability and conductivity. For example, the electrical conductivity of $TiO_2$ is $10^{-8}$ $S m^{-1}$ whereas TiN $4.5 \times 10^6$ $S m^{-1}$. The enhanced electronic conductivity of metal nitrides has in fact made it appealing for SC applications.

Despite its several advantages, metal nitrides exhibit poor rate capability, low charge storage capacity, and limited cycle life.[20] To (i) enhance the cycle life, (ii) expand the working potential window, and (iii) ensure outstanding rate capability, there is value for exploration of novel materials in SC

[a] U. N. Kumar, S. Ghosh, Dr. T. Thomas
Department of Metallurgical and Materials Engineering
Indian Institute of Technology Madras
Chennai, 600036, Tamil Nadu, India
E-mail: tijuthomas@iitm.ac.in
[b] J. N. Ramavath, S. Ghosh, Dr. R. Kothandaraman
Department of Chemistry,
Indian Institute of Technology Madras
Chennai, 600036, Tamil Nadu, India
E-mail: rkraman@iitm.ac.in

Supporting information for this article is available on the WWW under https://doi.org/10.1002/batt.201900225

technology. Recently, metal oxynitrides (MONs) have emerged as an intermediate family of compounds between metal oxides (MOs) and metal nitrides (MNs).[16] These metal oxynitrides are promising due to their rather large electronic conductivity (4000–55,500 $S\,cm^{-1}$), improved wettability (to the electrolyte), corrosion resistance, and bio-compatibility.[21,22] Some of these improved properties of MONs enable them to overcome issues associated with MOs such as volume expansion during cycling (which in turn leads to structural degradation).

In this context, various MONs have been reported; for instance, Wang et al.[23] synthesized various oxynitride layers MON (M=Fe, Co, Ni, V), which are grown on corresponding oxide materials to overcome the volume expansion and associated issues. It is the oxynitride overlayer that is shown to improve the cyclic stability. Another relevant study is by Yu et al.,[19] reported the outstanding cyclic stability ~$10^5$ cycles is exhibited by tungsten oxynitride (WON) fibers. Wang Z et al.[24] reported nanogrid film morphology of titanium oxynitride (TiON) which exhibits superior cyclability and capacitance retention.

The uses of transition metals (TMs) are crucial in SC technology due to their variable oxidation states. Among the TMs; Ni, Co, V, Ti are most widely explored for the development of electrode material for SCs. Chromium based compounds, while having been explored for optoelectronics, Micro-Electro-Mechanical systems (MEMS),[25] LIBs,[26,27] superconductors[28] and electrocatalysts;[29,30] it is largely under-explored for SC applications. The appeal for Cr compounds arise out of their (i) variable oxidation states, (ii) stability at high temperature, and (iii) corrosion resistant properties of Cr.[31,32] These offer desirable features of relevance to SCs as well. Particularly CrN and $Cr_2O_3$ are likely interesting from the standpoint of SC materials. However, from literature, we gather that the main concerns for these materials are: (i) low specific capacitance,[33,34] (ii) poor cyclic stability and rate capabilities, and (iii) low energy density.[34]

Hence, oxynitride phases may be considered as a plausible materials family that offers a means of overcoming existing barriers with pure Cr oxide and nitride phases. In principle, we anticipate that upsurge in electronic conductivity of chromium oxynitride ($CrO_XN_Y$) compared to its counterparts might improve the rate capability with good cyclic stability. In this context, to investigate the electrochemical performance of the $CrO_XN_Y$ for SC applications we have carried out three electrode and two measurements. Finally, a symmetric device is fabricated to evaluate cyclic stability, energy and power density in the view of real practical application.

## Experimental Section

### Chemical and reagents

All chemicals and reagents are used without further purification. Chromium chloride hexahydrate ($CrCl_3.6H_2O$), Urea ($CH_4N_2O$), N-methyl-2-pyrrolidone (NMP), poly(vinylidenefluoride) (PVDF), acetylene black, and potassium hydroxide (KOH) pellets are procured from Sigma Aldrich, India. Ethanol ($C_2H_5OH$) is purchased from Alfa Aesar and Nickel foam (Thickness: 2–3 mm and pore size 0.05–0.5 mm) is procured from Nanoshel, USA.

### Synthesis of $CrO_XN_Y$ active material

In this work, a soft-urea method is used to synthesize $CrO_XN_Y$ nanoparticles. To brief, chromium chloride and urea (1:5 mole ratio) is dissolved slowly in ethanol for 2 h with continuous stirring at room temperature. Further, this resulted mixture is stirred for 2 more hours to dissolve urea completely and then residual ethanol is removed by drying this solution at 120 °C. Finally, the obtained product is calcined at 800 °C for 3 h in Argon atmosphere. After furnace is cooled down to room temperature, $CrO_XN_Y$ are collected and then subjected to structural, morphological and electrochemical characterization to probe its properties. The schematic is shown in Figure 1 clearly represents the synthesis procedure of $CrO_XN_Y$. For comparison we prepared $Cr_2O_3$ (1:1 molar ratio) and CrN (1:6 molar ratio) using a similar method. Calcination temperature optimization is also performed. It is found that 800 °C is the optimum temperature for obtaining $CrO_XN_Y$ nanospheres.

### Physical characterization

The obtained $CrO_XN_Y$ are structurally characterized using Brukar X-ray diffractometer (XRD) using Cu $K_\alpha$ (1.5418 Å) to confirm the phase and crystallite size. X-ray photoelectron spectroscopy (XPS)

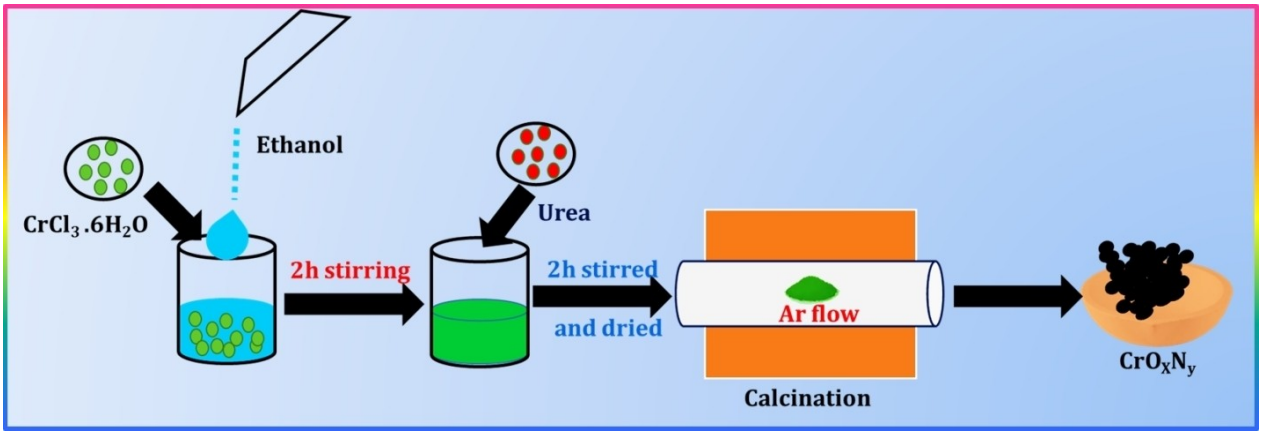


**Figure 1.** Schematic of step-wise synthesis of $CrO_XN_Y$ nanoparticles through soft urea method.

is used to evaluate the nitrogen doping, and also to get valance state of chromium in $CrO_XN_Y$, using OMICRON (Nano Technology Ltd.) fitted with Al $K_\alpha$ X-ray source. The surface area and pore size distribution of $CrO_XN_Y$ characterized by using micrometrics ASAP 2020 instrument. A high resolution XPS spectrum is recorded at the pass energy of 20 eV and high ultra-vacuum ($10^{-8}$ to $10^{-9}$) is maintained to generate X-ray with an electrical input of 15 kV and 20 mA. The resulting binding energies are calibrated with C 1s peak (284.8 eV). Morphological studies carried out using the FEI Quanta 400 scanning electron microscope (SEM) and Technai transmission electron microscope (TEM). In addition to all, CHNS analysis is done to the sample to quantify nitrogen percentage in $CrO_XN_Y$.

### Electrochemical characterization

$CrO_XN_Y$ (75 wt%), acetylene black (20 wt%) and PVDF (5 wt%) were ground well, and the slurry is prepared using NMP. Prior to the coating of active material, Ni foam is washed with 3 M HCl solution followed by distilled water and ethanol to remove the surface oxide layer, then dried at 60 °C for 6 h. Further, the prepared slurry is coated over Ni foam with active mass loading of 2 mg cm$^{-2}$ and dried at 80 °C overnight. The electrochemical characterization is carried out using Biologic Science potentiostat (SP-150) in three electrode set up with active material, Pt mesh and Hg/HgO as working, counter and reference electrodes respectively in 3 M KOH solution. Cyclic voltammetry (CV) and galvanostatic charge discharge (GCD) measurements are done in the potential range of −1.1 to −0.1 *V vs.* Hg/HgO in three-electrode cell at different scan rates (10-50 mV s$^{-1}$) and current densities (1–10 A g$^{-1}$). Electrochemical impedance spectroscopy (EIS) of $CrO_XN_Y$ and $Cr_2O_3$ samples is measured in three electrode configuration in the range of 1 Hz to 100 kHz.

### Symmetric device fabrication

Symmetric SC device is fabricated using coin cell (CR2032) and evaluated in two-electrode configuration. The symmetric device comprises of $CrO_XN_Y$/Ni foam as both the positive and negative electrode, and anion exchange membrane (AEM, Selemion AMV-N, 110 μm) is used as a separator. All electrochemical measurement of the symmetric SC device is done using AEM after soaking into 3 M KOH electrolyte solution for 24 h at room temperature. To understand charge transfer, mass transport characteristics of symmetric SC device the EIS study is carried out at open circuit voltage (0.182 V) in the frequency range of 0.01 to 100 kHz and the amplitude is 5 mV.

The gravimetric specific capacitance ($C_{3E}$) of electrode in three-electrode cell is calculated from Eq. (1)

$$C_{3E} = \frac{I\Delta t}{m\Delta V} \tag{1}$$

Where $I$ (in A) – applied current, $\Delta t$– discharge time, m (in g) – mass of the $CrO_XN_Y$ on the working electrode, $\Delta V$ (in V) – potential range. The gravimetric specific capacitance of single electrode ($C_{2E}$) in two-electrode mode is calculated using Eq. (2)

$$C_{2E} = \frac{4.I.\Delta t}{m_{tot}.\Delta V} \tag{2}$$

$m_{tot}$ (in g) – the total mass of the active material of both the electrodes

The specific energy density (Wh Kg$^{-1}$) and power density (W Kg$^{-1}$) of the symmetric cell are estimated based on the following Eqs. (3) and (4)

$$E = \frac{C_{2E}\Delta V^2}{28.8} \tag{3}$$

$$P = \frac{E}{\Delta t} \tag{4}$$

## 2. Results and Discussion

The phase, crystal structure, and crystallite size of synthesized $CrO_XN_Y$ are confirmed from XRD pattern, as shown in Figure 2a. From the XRD studies, it revealed that the existence of CrN phase with some traces of $Cr_2O_3$ phase. The XRD patterns corresponding to the peaks with 2θ angles at 37.46°, 43.62°, 63.29°, 76.02° and 80.07° and their corresponding Bragg's planes at (111), (002), (022), (113) and (222) indicates the presence of CrN (ICDD No: 98-004-7754). Similarly, the characteristic peaks with 2θ values and corresponding planes at 33.54°, 36.14°, 50.18°, and 54.80° and (104), (110), (024), and (116) indicates the presence of $Cr_2O_3$ phase, respectively (ICDD No: 98-001-1922). Hence, in the case of $CrO_XN_Y$ it is observed that the presence of a mixture of both CrN and $Cr_2O_3$ phases reveals that the successful formation of chromium oxynitride phase. The well-defined XRD pattern of $CrO_XN_Y$ is in well agreement with previous reports.[35] Further, from the Rietveld refinement (Figure S1) the lattice parameter of $CrO_XN_Y$ phase is found to be 4.152 Å.

The CHNS analysis of the $CrO_XN_Y$ is carried out to quantify the amount of nitrogen and oxygen in the sample. The N content of the sample found to be 2.40 (wt%) respectively. The morphology of the synthesized $CrO_XN_Y$ is analyzed using SEM micrograph. The SEM image shows uniformly distributed nano-spherical nanoparticles with little agglomeration throughout the sample (shown in Figure 2b). Elemental atomic percentage as derived from energy dispersive spectroscopy (EDS) mapping shows the presence of a significant amount of nitrogen (Figure S2) in the material.Calcination temperature dependent morphology studies are also conducted and corresponding micrographs are presented in Figure S4.It is concluded that 800 °C is the optimum temperature to obtain $CrO_XN_Y$ nano-spheres. To get high resolution morphology of $CrO_XN_Y$ TEM studies are done. TEM micrographs also show that the presence of nanostructured and nano-spherical morphology of $CrO_XN_Y$ varying the size from 18 to 25 nm as shown in Figure 2c. Figure 2d indicates the typical diffused ring pattern of $CrO_XN_Y$ with cubic crystal structure in the selected area electron diffraction (SAED) pattern. The surface area and porosity of the $CrO_XN_Y$ are evaluated by Brunauer-Emmett-Teller (BET) and Barrett-Joyner-Halenda (BJH) methods. The nitrogen adsorption-desorption plot (Figure 3a) of the sample revealed that $CrO_XN_Y$ exhibits a typical mesoporous nature. The BET surface area of the active material is found to be 34 m$^2$ g$^{-1}$ with an average pore diameter of 21 nm.

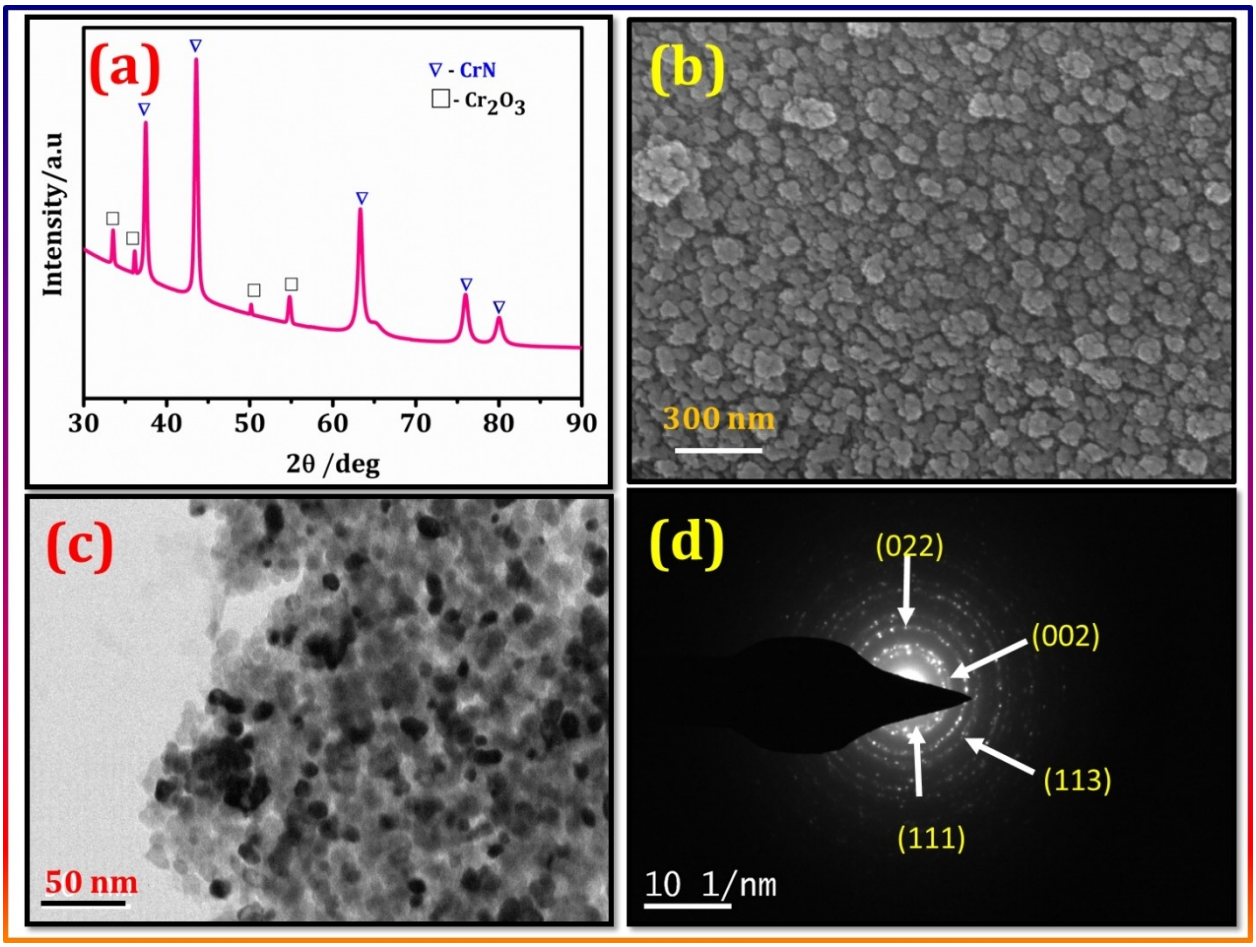


**Figure 2.** a) XRD pattern of $CrO_XN_Y$,b) Morphology of as-synthesized $CrO_XN_Y$ which shows nano spherical morphology with little agglomeration, c) high-resolution TEM micrographs of $CrO_XN_Y$, d) selected area electron diffraction (SAED) pattern of $CrO_XN_Y$ exhibiting the diffused rings with cubic structure.

In addition to this, X-ray photoelectron spectroscopy (XPS) is carried out to estimate the valence state and binding energies of Cr, O, and N in the resulting $CrO_XN_Y$phase. The XPS survey spectrum of the sample is recorded in the range of 200 to 1000 eV, as shown in Figure 3b. Presence of two major peaks around 396 eV and 530 eV confirms the presence of both nitrogen and oxygen in the $CrO_XN_Y$material (as shown in Figure 3d & S3). The high resolution spectra of Cr $2P_{3/2}$ display three peaks at 576.16, and 578.36 eV indicates the presence of Cr–N and Cr–O respectively (as shown in Figure 3c).Similarly, the deconvolution spectra of N 1s shows three peaks at 396.6 and 398.8 eV (Figure 3d) indicates presence of Cr–N and Cr–N–O bonding, respectively.[36] Finally, from Cr $2p_{3/2}$ spectrum, it also reveals that Cr exhibit +3 oxidation state in $CrO_XN_Y$. From the Cr $2p_{3/2}$, O 1s and N 1s spectra it infers that the formation of the $CrO_XN_Y$ phase.

To investigate the electrochemical performance of $CrO_XN_Y$ is used as an active electrode in both three and two electrode assembly. Figure 4a.Shows three electrode CV profiles of $CrO_XN_Y$ at different scan rates from 10 to 50 mV $s^{-1}$. CV curves exhibit a typical rectangular behavior at all the scan rates indicates that the mainly EDLC behavior of the materials in the working voltage window of−1.1 to−0.1 Vvs. Hg/HgO. The specific capacitance in three-electrode configuration ($C_{3E}$) at low scan rate (10 mV $s^{-1}$) is found to be 146 F $g^{-1}$ and at high scan rate (50 mV $s^{-1}$), it is found to be 121 F $g^{-1}$. The retention of quasi rectangular CV curve with ~83% capacity retention even at high scan rate (50 mV $s^{-1}$) compared to lower scan rate (10 mV $s^{-1}$) indicates that $CrO_XN_Y$ can act as the potential electrode material for SC applications. The obtained capacitance of $CrO_XN_Y$ electrode is much higher than previously reported chromium oxide ($Cr_2O_3$) and chromium nitride (CrN). For instance, M. Arif et al.[34] reported sputter coated thin film of CrN, which has the specific capacitance of 41.6 F $g^{-1}$ at 5 mV $s^{-1}$ in 1 M $Na_2SO_4$. In this study also, we have synthesized $Cr_2O_3$ and CrN using similar method (calcined @ 800 °C). From CV profiles, it is clear that $CrO_XN_Y$ electrode materials exhibit far better SC performance with specific capacitance ($C_{3E}$) of 125 F $g^{-1}$ @ 30 mV $s^{-1}$. This is betterthan the case with the oxide (37 F $g^{-1}$) and nitride (94 F $g^{-1}$) in the same working potential range (shown in Figure S7). The impressive capacitive nature of $CrO_XN_Y$ is plausibly due to the presence of a mixture of phases (as indicated in Figure 2a &Figure S1) and low charge transfer resistance.

The morphology and structure can influence the charge storage behavior of corresponding MON. In this study, obtained

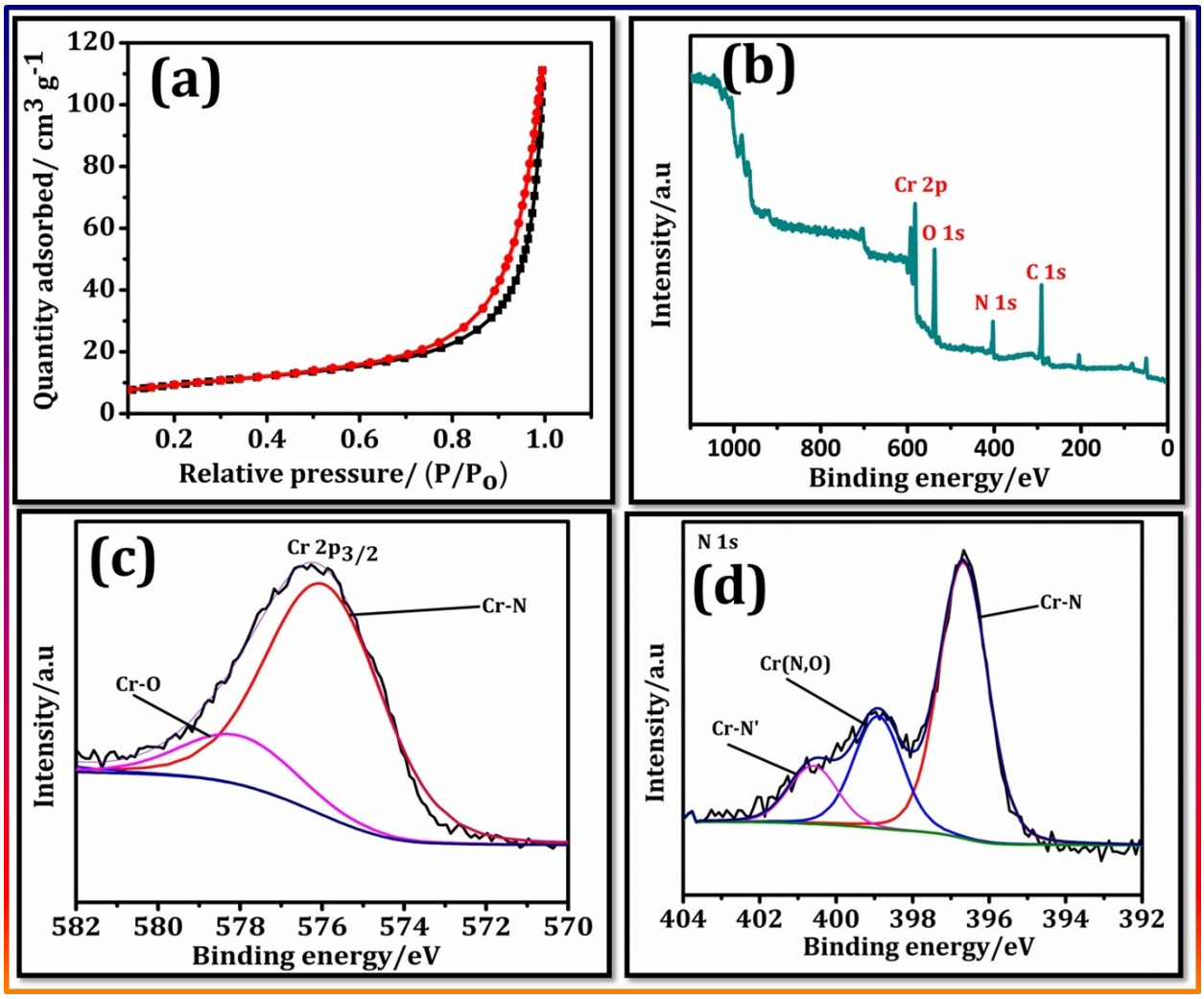


**Figure 3.** a) Nitrogen adsorption-desorption curves for$CrO_XN_Y$ from BET mesurements, b) XPS survey spectrum of $CrO_XN_Y$,c) deconvoluted XPS spectrum of Cr $2p_{3/2}$, confirm the oxidation state of Cr is +3, d) deconvoluted XPS spectrum of N 1s, which comprises of Cr–N and Cr (N,O) binding energies.

$CrO_XN_Y$ nanospheres are one of favorable nanostructures for better electrochemical properties.[37] Based on the presence of the type of metal present in oxynitride, the charge storage behavior of MON can be either EDLC or PSC.[20] Y. Yang et al. conducted CV measurements in three electrode configuration for highly ordered porous/tubular $VO_xN_y$ layers in the range of −1.2 to 0 *V*s. Ag/AgCl. The $VO_xN_y$ shows the capacitance of 250 $F\,g^{-1}$ at 2 $mV\,s^{-1}$ in 1 M KOH. It is also observed that $VO_xN_y$ stores energy via pseudo-capacitive mechanism due to typical redox features corresponding to various oxidation states of vanadium.[38] Dong Shu et al. reported that the presence of redox peaks results pseudo-capacitive charge storage mechanism of Vanadium oxynitride-carbon ($VO_xN_y$–C) electrode in 1 M KOH. The $VO_xN_y$–C electrode exhibited a higher capacitance value (271 $F\,g^{-1}$) than $VO_xN_y$ (143 $F\,g^{-1}$) at 1 $A\,g^{-1}$. It is reported that the enhanced capacitance of $VO_xN_y$–C is due to improved conductivity and surface area compared to $VO_xN_y$.[39] Kartachova et al. reported that tungsten oxynitride (WON) stores the energy via EDLC mechanism in 1 M $H_2SO_4$.[15]

The WON electrode shows the capacitance of 85 $F\,g^{-1}$ at 0.05 $A\,g^{-1}$ in 1 M $H_2SO_4$ and 57 $F\,g^{-1}$ at 0.5 $A\,g^{-1}$ in 1 M KOH.[15] It is evident from previous literature that most of the MONs (M=Ti, Mo, W and V) store charges at the interface via double layer formation and/or a fast reversible redox reaction [Eq. (5)].[20] From the quasi-rectangular CV profiles (Figure 4a), it is understood that $CrO_XN_Y$ stores charges via electric double layer formation. Hydroxyl ions from electrolyte are adsorbed at the electrode surface during charging and form the electric double layer at the $CrO_XN_Y$ interface. During discharge, the adsorbed hydroxyl ions diffuse into the electrolyte from the electrode surface. However presence of broad redox peaks due to Faradic reactions indicate electron transfer across the double layer, which lead to the formation of $CrO_XN_Y$–OH species.[40] The possible mechanism of energy storage via double layer formation is given in Eq. (5)

$$CrO_XN_Y + OH^- \leftrightarrow CrO_XN_Y\,||OH^- + CrO_XN_Y - OH \quad (5)$$

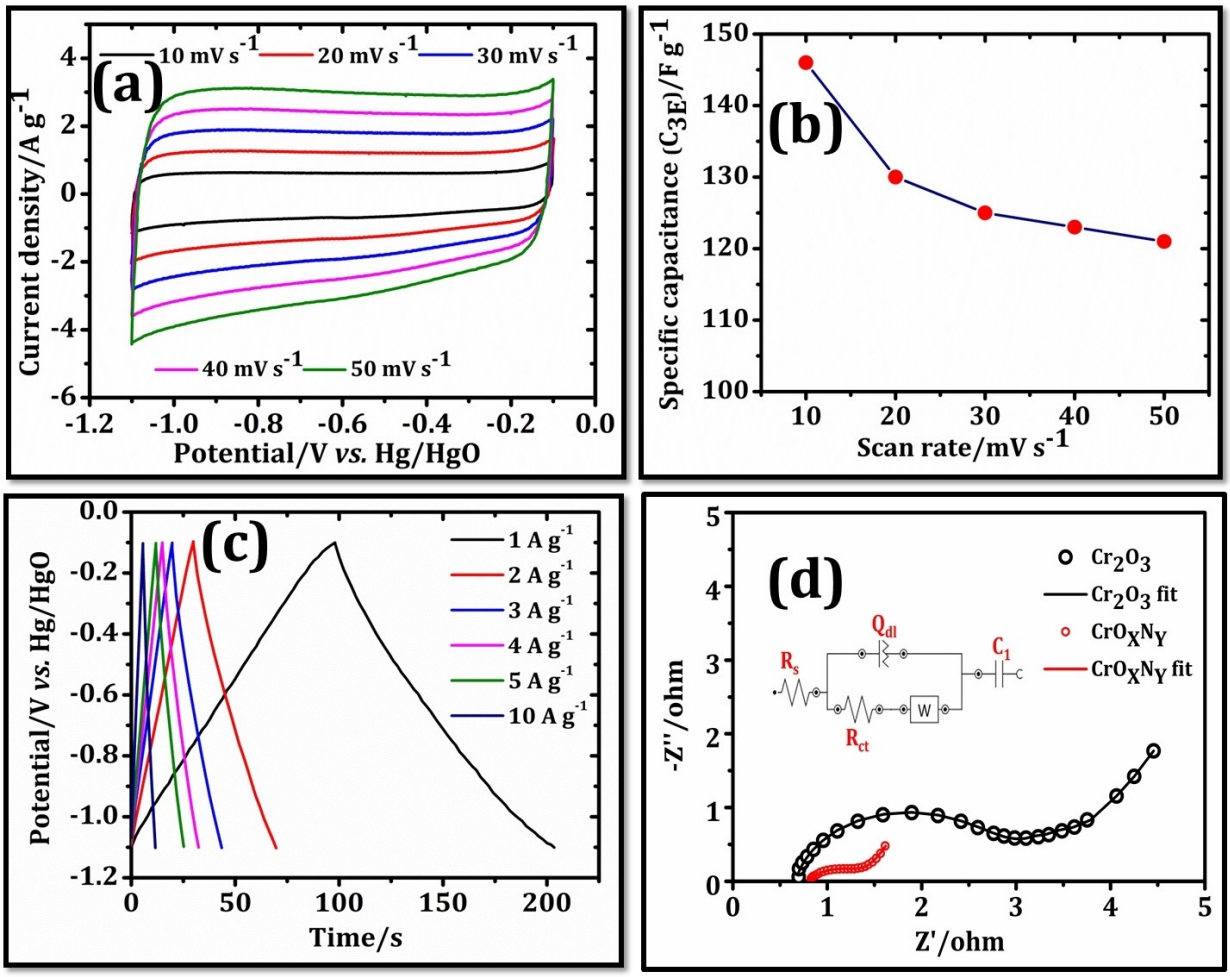


**Figure 4.** Electrochemical characterization in three electrode assembly a) CV curves of$CrO_XN_Y$ at different scan rates (10–50 mV $s^{-1}$), b) specific capacitanc at different scan rate, which decrease with incresing the scan rates, c) Galvanostatic charge discharge curves at different current densities, d) Nyquist plots of both $CrO_XN_Y$ and $Cr_2O_3$ fitted with equivalent circuit

It can be noted that the electrochemical stability of most of the MON (M=V, W, and etc.,) strongly depends on the lower and upper potential limits. Porto et al. reported that VN29 ($VO_xN_y$) electrode exhibited good electrochemical stability in the range of−1.2 to 0 V than−1.2 to−0.4 *V*vs. Hg/HgO.[41] When the high potential limit is used, irreversible oxidation occurs, and dissolution of vanadium from VOxNy electrode results in the formation of soluble vanadium based species causes capacity fade of the electrode during cycling. Restricting the potential limits improves the cyclic stability of VOxNy but decreases the energy density of the SCs.[39] The enhancement in the upper and lower potential limits of the electrode material can greatly enhance the energy density of the SC.

Interestingly, and mirroring these trends; $CrO_XN_Y$ shows good electrochemical stability in the range of−1.1 to−0.1 *V*vs. Hg/HgO in 3 M KOH. The variation of $C_{3E}$ of $CrO_XN_Y$ electrode at different scan rate is displayed in Figure 4b. It can be seen that ~83% of capacity retention even at high rate (50 mV s−1) indicates excellent electrochemical reversibility and rate capability of the $CrO_XN_Y$ electrode in 3 MKOH. Figure S6 show CV curves of $CrO_XN_Y$ electrodes which are synthesized at different calcination temperatures. The specific capacitance of the 3 electrode system, designated as $C_{3E}$ value, for $CrO_XN_Y$−700, $CrO_XN_Y$−800 and $CrO_XN_Y$−900 are 70 F $g^{-1}$, 125 F $g^{-1}$ and 50 F $g^{-1}$respectively. The high capacitance of $CrO_XN_Y$−800 is likely due to exact phase formation at this optimum temperature. Hence we have carried out systematic studies with $CrO_xN_y$−800 material. The EIS Nyquist plots of $CrO_XN_Y$ and $Cr_2O_3$ electrodes are shown in Figure 4d. Inset to the Figure 4d shows that equivalent circuit that is used to fit the Nyquist curves obtained. The EIS spectra of the $CrO_XN_Y$ and $Cr_2O_3$ electrodes show a broad semicircle at high frequency corresponding to the region of charge transfer kinetics. A middle frequency region with 45° slope indicates a diffusion limited process and a straight line at low frequency corresponds to capacitive response of the system. From the fitting circuit, $R_s$ and $R_{ct}$ are the bulk solution resistance and charge transfer resistance, respectively. The $Q_{dl}$ (is a constant phase element) and C1 describes the EDLC and Faradaic pseudo-capacitance, respectively. W corresponds to Warburg impedance, which is related to the transfer of ions from the bulk electrolyte to the electrode surface.[42] The $R_{ct}$ value for $CrO_XN_Y$ (0.60 Ω) is much lower than

that of $Cr_2O_3$ (2.29 Ω) electrode (Figure 4d). The smaller $R_{ct}$ of $CrO_XN_Y$ indicates rather rapid ion diffusion into mesopores of the electrode material. The equivalent circuit based analysis indicates that N doping in the $Cr_2O_3$ phase not only improves $CrO_XN_Y$ conductivity but also lowers the interfacial charge transfer resistance, which in turn ensures fast charge transport process even at high rates.

To examine the electrochemical response of $CrO_XN_Y$ electrode in the given potential range galvanostatic charge-discharge (GCD) studies are carried out at different current density values in the three-electrode configuration as shown in Figure 4c. From the GCD it is observed that all the GCD curves show a triangular shape profiles indicates that the $CrO_XN_Y$ exhibits close to ideal capacitive nature at all current densities. The rate capability is tested at different current densities varies from 1 to 10 $A\,g^{-1}$. The $C_{3E}$ at 1,2,3,4,5 and 10 $A\,g^{-1}$are 105,80,69,68,65 and 60 $F\,g^{-1}$ respectively. B Wei et al.[43] reported DC magnetron sputter coated CrN exhibits areal capacitance of 12.8 $mF\,cm^{-2}$ at 1.0 $mA\,cm^{-2}$. The enhancement of the capacitance of $CrO_XN_Y$ compared to earlier reported chromium nitride phases could be due to improved charge storage and good electronic conductivity of $CrO_XN_Y$ phase. On the other hand, the electrode and electrolyte interaction plays an important role in the charge storage behavior of $CrO_XN_Y$ electrode. In general, the electric conductivity of the electrode and ionic transport nature of electrolyte to the surface of the electrode matters a lot for judging the capacitive performance of the electrode. At low current density, $CrO_XN_Y$ shows high gravimetric capacitance (105 $F\,g^{-1}$, 1 $A\,g^{-1}$) compared to high current density (60 $F\,g^{-1}$, 10 $A\,g^{-1}$). This is due to sufficient time is offered for the ions to diffuse towards the electrode surface in the former case compared to later.

The observed features of $CrO_XN_Y$implies that it is a reasonable material for fabricating a SC device. A symmetric device is made using a coin cell (CR2032) where $CrO_XN_Y$ of equal mass loading is used as a positive and negative electrode. The KOH soaked anion exchange membrane (Selemion AMV–N, 110 μm) is used as a separator. The electrochemical performance of the symmetric device characterized by CV and GCD measurements in the working voltage range of 0–1 V. The CV studies at lower (10–50 $mV\,s^{-1}$) and higher scan rates (100–500 $mV\,s^{-1}$) of the symmetric cell are depicted in Figure 5a and 5b. The symmetric device shows 146 $F\,g^{-1}$ at a low scan rate (5 $mV\,s^{-1}$) and 83 $F\,g^{-1}$ at high scan rate (500 $mV\,s^{-1}$).[44] Nearly ~57% of capacity retention is observed even at higher scan rates. It is also observed that the symmetric device still maintained nearly rectangular CV profiles up to 50 $mV\,s^{-1}$. From the CV profiles (Figure 5a and 5b), it is clear that even at high rates $CrO_XN_Y$ shows quasi rectangular shape; this indicates that good rate capability. Further to have better insight into the mechanism of charge storage of $CrO_XN_Y$ NPs, the capacitive contributions from electrical double layer capacitance (EDLC) and pseudo-capacitance (PSC) to the total capacitance were quantified using Eq. (6) at various sweep rates.

$$\mathbf{i}(\mathbf{V}) = \mathbf{k}_1\mathbf{v} + \mathbf{k}_2\mathbf{v}^{0.5} \quad (6)$$

Here the constants $\mathbf{k}_1$ and $\mathbf{k}_2$ represent contributions to the capacitance. As it is evident from the previous reports, for a surface controlled process, current response ($\mathbf{i}(\mathbf{V})$) varies linearly with scan rate ($\mathbf{v}$) whereas it varies linearly with square root of scan rate ($\mathbf{v}^{0.5}$) for pseudo-capacitive process or semi-infinite diffusion process.[45] From Figure 5a, we notice that at low scan rates (5 $mV\,s^{-1}$), the percentage of contribution of EDLC and PSC to the total capacitance are 70% and 30% respectively. Even at high scan rate (50 $mV\,s^{-1}$), the percentage of contribution of EDLC and PSC are found to be 88% and 12% respectively. From this it is clear that to the total capacitance, EDLC contribution is much higher than that of PSC. Hence it can be envisaged that $CrO_XN_Y$ NPs stores charge primarily via the EDLC mechanism. More specifically, it is likely that the oxide rich phase (as indicated by Rietveld refinement) contributes to PSC, while the nitride rich phase contributes to EDLC, which is the dominant mechanism. The GCD measurement at different current densities (0.5–10 $Ag^{-1}$) is carried out for symmetric SC, as shown in Figure 5c. All the GCD curves show linear charge-discharge profiles indicate that EDLC mechanism of energy storage of the $CrO_XN_Y$ electrode.

The Nyquist plot of the symmetric SC device is shown in Figure 5d. The small $R_{ct}$ value ~0.9 Ω of symmetric device shows fast charge transport nature of the fabricated coin cell device. At low frequencies, $CrO_XN_Y$ shows approximately vertical straight line parallel to the Y-axis; this indicates good capacitance characteristics of the symmetric SC device. The lower $R_{ct}$ from the SC device indicates faster ion diffusion and enhanced electrical conductivity of $CrO_XN_Y$ material. These are likely the favorable factors that enable the high rate capabilities of the fabricated device, even after 10,000 charge/discharge cycles.

The cyclic stability of symmetric SC device is tested over 10,000 cycles at 2 $A\,g^{-1}$. Even after 10,000 charge/discharge cycles, the $CrO_XN_Y$ exhibits excellent capacity retention of 98%. The retaining of its initial capacitance over long term 10,000 charge/discharge cycles indicates good cyclic stability of the electrode. The observed specific surface area, mesoporosity and structural robustness of as-prepared $CrO_XN_Y$ electrode material enable capacitance retention of ~98%. Furthermore Coulombic efficiency of ~99% after 10,000 charge/discharge cycles are observed, as shown in Figure S5. The structural and surface features of $CrO_XN_Y$ nanospheres provide ionically accessible sites for ion transportation. This results in good rate capability and cyclic stability of the electrode material. Hence, we believe that $CrO_XN_Y$ electrode can be a suitable promising electrode material for SC applications due to its excellent cyclic stability and durability. The present work is compared in terms of capacity retention and cyclic stability with various oxynitrides and nitrides reports as given in the Table S1.The energy density and the power density of the symmetric SC device are ~8 $Wh\,kg^{-1}$ (at 1 $A\,g^{-1}$) and 28.8 $kW\,kg^{-1}$(at 10 $A\,g^{-1}$) respectively. As a proof of concept we have demonstrated that light emitting diode (LED) is lit with the serially connected two symmetric coin cell devices having the resultant voltage of 2 V as shown in the Figure 5e. These results suggest that $CrO_XN_Y$ can be the suitable electrode material having excellent

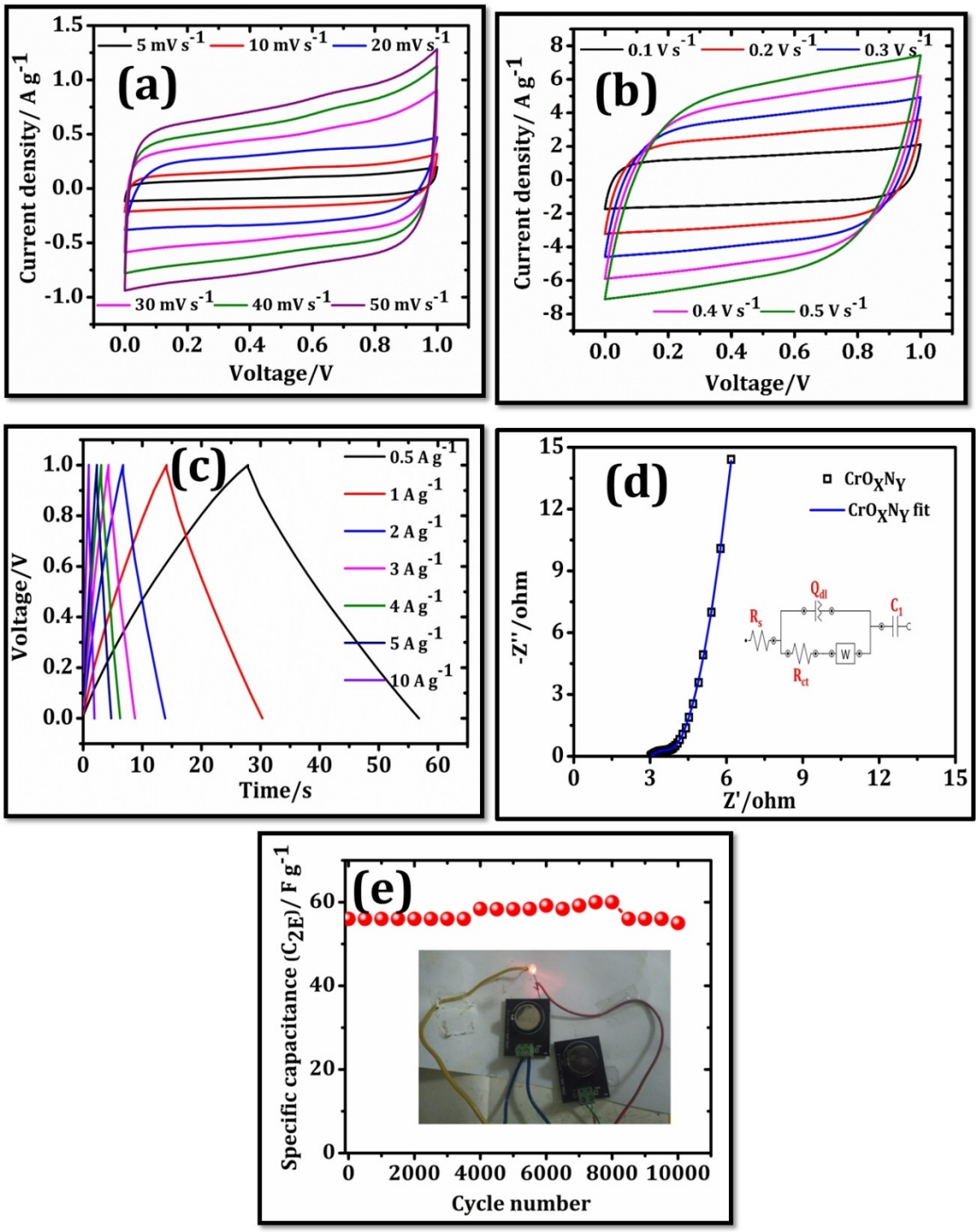


**Figure 5.** Electrochemical characterization of symmetric cell (coin cell). a) CV studies of$CrO_XN_Y$ at lower scan rates (5–50 mV $s^{-1}$), b) CV curves at higher scan rates (100–500 mV $s^{-1}$), c) GCD curves at different scan rates. d) Nyquist plot of symmetric device fitted with equivalent circuit, e) cyclic stability (up to 10,000) and capacitance retention(98 %) plot, as proof of concent LED was glowed using two coin cells in series connection.

capacitive retention and durability for SC applications operating in 3 M KOH aqueous medium.

## 3. Conclusions

In this study, $CrO_XN_Y$ are synthesized using an easy and scalable soft urea method. Further, these $CrO_XN_Y$ subjected to both physical and electrochemical characterization. The formation of oxynitride phase is confirmed through XRD, XPS, and CHNS analyzer. Further, electrochemical studies reveal that $CrO_XN_Y$

exhibit a maximum specific capacitance ($C_{3E}$) of 146 $F g^{-1}$ at 10 $mV s^{-1}$ in three-electrode cell. The cyclic stability (up to 10,000 cycles), capacitance retention (up to 98%) and high rate capability of resulting symmetric device proves its potential as SC device. Apart from that high energy density (8 $Wh kg^{-1}$), power density (28.8 $kW kg^{-1}$), and low solution resistance of the symmetric device makes it a prospective candidate for SCs application. These outcomes confirm that $CrO_XN_Y$could be a promising electrode material for high-rate capable and durable supercapacitor applications.

## Acknowledgment

*U. Naveen Kumar, Janraj Naik Ramavath, and Sourav Ghosh greatly acknowledge the help from HTRA fellowship of IIT Madras Authors also acknowledge the Prof. T Pradeep from Department of Chemistry, IITM for the XPS measurements. Also they, convey their gratitude to the Department of Metallurgical and Materials Engineering, Department of Chemistry, IITM.*

## Conflict of Interest

The authors declare no conflict of interest.

**Keywords:** chromium · durability · rate capability · oxynitride · symmetric supercapacitor

[1] A. Berrueta, A. Ursua, I. S. Martin, A. Eftekhari, P. Sanchis, *IEEE Access* **2019**, *7*, 50869.
[2] X. Zhao, B. M. Sánchez, P. J. Dobson, P. S. Grant, *Nanoscale* **2011**, *3*, 839.
[3] B. D. Patrice Simon, Y. Gogotsi, *Mater. Sci.* **2014**, *343*, 1210.
[4] P. Simon, Y. Gogotsi, *Nat. Mater.* **2008**, *7*, 845.
[5] R. Dubey, V. Guruviah, *Ionics* **2019**.
[6] C. qi Yi, J. peng Zou, H. zhi Yang, X. Leng, *Trans. Nonferrous Met. Soc. China* **2018**, *28*, 1980.
[7] G. Wang, L. Zhang, J. Zhang, *Chem. Soc. Rev.* **2012**, *41*, 797.
[8] N. Jäckel, P. Simon, Y. Gogotsi, V. Presser, *ACS Energy Lett.* **2016**, *1*, 1262.
[9] J. N. Ramavath, M. Raja, S. Kumar, R. Kothandaraman, *Appl. Surf. Sci.* **2019**, *489*, 867.
[10] P. Venkateswarlu, E. Umeshbabu, U. N. Kumar, P. Nagaraja, P. Tirupathi, G. Ranga Rao, P. Justin, *J. Colloid Interface Sci.* **2017**, *503*, 17.
[11] V. Augustyn, P. Simon, B. Dunn, *Energy Environ. Sci.* **2014**, *7*, 1597.
[12] M. K. Sahoo, G. Ranga Rao, *Electrochim. Acta* **2018**, *268*, 139.
[13] A. N. Grace, R. Ramachandran, M. Vinoba, S. Y. Choi, D. H. Chu, Y. Yoon, S. C. Nam, S. K. Jeong, *Electroanalysis* **2014**, *26*, 199.
[14] D. Choi, G. E. Blomgren, P. N. Kumta, *Adv. Mater.* **2006**, *18*, 1178.
[15] O. Kartachova, A. M. Glushenkov, Y. Chen, H. Zhang, X. J. Dai, Y. Chen, *J. Power Sources* **2012**, *220*, 298.
[16] U. N. Kumar, S. Ghosh, T. Thomas, *ChemElectroChem* **2019**.
[17] I. Shown, A. Ganguly, L.-C. Chen, K.-H. Chen, *Energy Sci. Eng.* **2014**, *3*, 2.
[18] P. Syedvali, G. Rajeshkhanna, E. Umeshbabu, G. U. Kiran, G. Ranga Rao, P. Justin, *RSC Adv.* **2015**, *5*, 38407.
[19] M. Yu, Y. Han, X. Cheng, L. Hu, Y. Zeng, M. Chen, F. Cheng, X. Lu, Y. Tong, *Adv. Mater.* **2015**, *27*, 3085.
[20] S. Ghosh, S. M. Jeong, S. R. Polaki, *Korean J. Chem. Eng.* **2018**, *35*, 1389.
[21] T. T. Chen, H. P. Liu, Y. J. Wei, I. C. Chang, M. H. Yang, Y. S. Lin, K. L. Chan, H. T. Chiu, C. Y. Lee, *Nanoscale* **2014**, *6*, 5106.
[22] E. J. Lee, L. Lee, M. A. Abbas, J. H. Bang, *Phys. Chem. Chem. Phys.* **2017**, *19*, 21140.
[23] TMON - Transition-Metal Oxynitride; A Facile Strategy for Improving Electrochemical Capacitor Storage.pdf.
[24] Z. Wang, Z. Li, Z. Zou, *J. Power Sources* **2015**, *296*, 53.
[25] C. Constantin, M. B. Haider, D. Ingram, A. R. Smith, *Appl. Phys. Lett.* **2004**, *85*, 6371.
[26] Q. Sun, Z.-W. Fu, *Electrochem. Solid-State Lett.* **2007**, *10*, A189.
[27] Y. N. Zhou, Z. W. Fu, *Adv. Mater. Res.* **2011**, *295–297*, 912.
[28] M. Sluban, P. Umek, Z. Jagličić, J. Buh, P. Šmitek, A. Mrzel, C. Bittencourt, P. Guttmann, M. H. Delville, D. Mihailović, D. Arčon, *ACS Nano* **2015**, *9*, 10133.
[29] M. Yang, Z. Cui, F. J. Disalvo, *Phys. Chem. Chem. Phys.* **2013**, *15*, 7041.
[30] Y. Zhang, W. Qiu, Y. Ma, Y. Luo, Z. Tian, G. Cui, F. Xie, L. Chen, T. Li, X. Sun, *ACS Catal.* **2018**, *8*, 8540.
[31] M. Yang, A. J. Allen, M. T. Nguyen, W. T. Ralston, M. J. MacLeod, F. J. DiSalvo, *J. Solid State Chem.* **2013**, *205*, 49.
[32] N. D. Nam, D. S. Jo, J. G. Kim, D. H. Yoon, *Thin Solid Films* **2011**, *519*, 6787.
[33] X. Xu, J. Wu, N. Yang, H. Na, L. Li, J. Gao, *Mater. Lett.* **2015**, *142*, 172.
[34] M. Arif, A. Sanger, A. Singh, *Mater. Lett.* **2018**, *220*, 213.
[35] Y. Yao, Q. Feng, S. Zhu, J. Li, Y. Yao, Y. Wang, Q. Wang, M. Gu, H. Wang, H. Li, X. Yuan, M. Shao, *Small Methods* **2018**, *1800324*, 1.
[36] A. Lippitz, T. Hübert, *Surf. Coat. Technol.* **2005**, *200*, 250.
[37] Y. Liu, L. Liu, Y. Tan, L. Niu, L. Kong, L. Kang, F. Ran, *Electrochim. Acta* **2018**, *262*, 66.
[38] Y. Yang, R. Kirchgeorg, R. Hahn, P. Schmuki, *Electrochem. Commun.* **2014**, *43*, 31.
[39] D. Shu, H. Cheng, C. Lv, M. Abou, *Int. J. Hydrogen Energy* **39**, 16139.
[40] D. Choi, G. E. Blomgren, P. N. Kumta, *Adv. Mater.* **2006**, *18*, 1178.
[41] R. L. Porto, R. Frappier, J. B. Ducros, C. Aucher, H. Mosqueda, S. Chenu, B. Chavillon, F. Tessier, F. Cheviré, T. Brousse, *Electrochim. Acta* **2012**, *82*, 257.
[42] S. Ghosh, G. Ranga Rao, T. Thomas, *ChemistrySelect* **2020**, *5*, 1628.
[43] B. Wei, H. Liang, D. Zhang, Z. Wu, Z. Qi, Z. Wang, *J. Mater. Chem. A* **2017**, *5*, 2844.
[44] U. N. Kumar, T. Thomas, *Indian Patent Office*, Application No.**201941049990**.
[45] A. Chowdhury, R. Shukla, V. Sharma, S. Neogy, A. Chandra, V. Grover, A. K. Tyagi, *J. Alloys Compd.* **2020**, *829*, 154479.

Manuscript received: December 23, 2019
Revised manuscript received: March 17, 2020
Accepted manuscript online: March 18, 2020
Version of record online: April 3, 2020